European Journal of Pharmaceutical Sciences 220 (2026) 107483

Contents lists available at ScienceDirect

European Journal of Pharmaceutical Sciences

journal homepage: www.elsevier.com/locate/ejps

Lemon balm-derived nanovesicles restore mitochondrial function and reduce cytokine production in skin fibroblasts under pro-inflammatory conditions

Gabrielė Kulkovienė [a,b,*], Martyna Uldukytė [b], Sofiya Haluts [a], Emilija Mikalauskienė [b,c], Monika Iešmantaitė [d], Giedrė Tamulaitienė [e], Giedrius Sasnauskas [e], Ramunė Morkūnienė [a,1], Aistė Jekabsone [b,c,*,1]

[a] Department of Drug Chemistry, Faculty of Pharmacy, Lithuanian University of Health Sciences, Kaunas, 50166, Lithuania
[b] Laboratory of Pharmaceutical Sciences, Institute of Pharmaceutical Technologies, Lithuanian University of Health Sciences, Kaunas, 50166, Lithuania
[c] Preclinical Research Laboratory for Medicinal Products Institute of Cardiology, Lithuanian University of Health Sciences, Kaunas, 50166, Lithuania
[d] Department of Biological Models, Institute of Biochemistry, Life Sciences Center, Vilnius University, Vilnius, 10257, Lithuania
[e] Institute of Biotechnology, Life Sciences Center, Vilnius University, Vilnius, 10257, Lithuania

ARTICLE INFO

Keywords:
Plant-derived nanovesicles
Lemon balm
Mitochondria
Inflammation
Psoriasis
Atopic dermatitis

ABSTRACT

Mitochondrial dysfunction, particularly excessive fission, has been implicated in inflammatory signalling in skin diseases such as psoriasis and atopic dermatitis (AD). Current systemic treatments, while effective, are often associated with adverse effects, variable patient responses and high costs. Plant extracts have shown notable anti-inflammatory properties; however, their therapeutic potential is limited due to low penetration and poor bioavailability. Thus, plant-derived nanovesicles (PDNVs) have emerged as an alternative delivery platform, offering bioactive cargo with improved skin penetration and low immunogenic potential. *Melissa officinalis L.* (Lemon Balm, LB) extracts have demonstrated beneficial effects in inflammatory skin conditions; however, the potential of LB-NVs to modulate skin cell function and cellular energetics in inflammatory conditions remains unexplored. Thus, this study investigated the effects of LB-NVs on mitochondrial function and structure in human skin fibroblasts exposed to a cytokine cocktail (IL-22, IL-17A, TNF-α) to induce a pro-inflammatory state (PInfS). LB-NVs rescued cells from inflammatory metabolic reprogramming by restoring mitochondrial respiration and preventing elevated glycolysis induced by PinfS. Additionally, they reduced mitochondrial fragmentation by regulating the activation of Drp1 and lowered the total p38 MAPK level. Lastly, LB-NVs suppressed IL-4 and IL-13, which are central to AD pathogenesis, and reduced IL-18, a cytokine that commonly increases with disease activity. These findings, for the first time, demonstrate the ability of PDNVs to directly target mitochondrial functions and modulate inflammation, positioning LB-NVs as a highly promising strategy for treating chronic skin inflammation.

1. Introduction

Skin inflammatory diseases are characterised by an abnormal response of immune cells to endogenous or exogenous stimuli, leading to the onset and persistence of inflammation that often becomes a chronic state (Tampa et al., 2022). Fibroblasts, traditionally recognised as stromal cells, responsible for maintaining skin integrity, have emerged as key players in inflammatory processes (Chen et al., 2024). In psoriasis, as well as certain forms of atopic dermatitis (AD), IL-17A, TNF-α and IL-22 can activate fibroblasts, leading to immune cell recruitment

Abbreviations: AD, atopic dermatitis; Cryo-EM, cryo-electron microscopy; DW, dry weight; Drp1, Dynamin-related protein 1; ECAR, extracellular acidification rate; GDAP1L1, Ganglioside Induced Differentiation Associated Protein 1 Like 1; H_2O_2, Hydrogen peroxide; IL, interleukin; JAK, Janus kinase; IMQ, imiquimod; LB-NVs, Lemon balm-derived nanovesicles; MAPK, Mitogen-Activated Protein Kinase; NTA, nanoparticle tracking analysis; OCR, oxygen consumption rate; PDNVs, Plant-derived nanovesicles; PInfS, Pro-inflammatory state; ROS, reactive oxygen species.

* Corresponding authors.
E-mail addresses: gabriele.kulkoviene@lsmu.lt (G. Kulkovienė), aiste.jekabsone@lsmu.lt (A. Jekabsone).
[1] These authors contributed equally to this work.

https://doi.org/10.1016/j.ejps.2026.107483
Received 30 August 2025; Received in revised form 9 February 2026; Accepted 21 February 2026
Available online 23 February 2026

and perpetuation of chronic inflammation (Chen et al., 2024; Guttman-Yassky and Krueger, 2017). Understanding fibroblast-driven mechanisms may open new avenues for disease modulation.

The most advanced therapies for both psoriasis and AD are systemic biologics targeting key inflammatory cytokines and JAK inhibitors able to suppress many immune pathways (Greb et al., 2016; Jeskey et al., 2024). While these agents can be highly effective, their benefits are not uniform across patients, they can cause adverse effects and are associated with high treatment costs. Therefore, identifying novel therapeutic targets is essential for developing safer, more effective and accessible treatment options.

New findings indicate that mitochondrial dysfunction can have a significant impact on skin health and contribute to the progression of skin diseases. In macrophages, mitochondrial fission was shown to induce psoriasis-related cytokine production via fission regulators GDAP1L1 and Drp-1 (Alalaiwe et al., 2021). Elevated Drp1 expression has been reported in psoriatic lesional (Weng et al., 2020) and in AD skin (Zhang et al., 2011) and its inhibition has been shown to suppress disease symptoms in mouse models of AD and psoriasis (Alalaiwe et al., 2021; Li et al., 2021). Previous work demonstrated that inflammation resolution depended more on restoring the mitochondrial network than reducing reactive oxygen species in fibroblasts, highlighting mitochondrial dynamics as a potential therapeutic target (Kulkovienė et al., 2025).

Plant extracts are widely recognised for their anti-inflammatory and antioxidant properties and have shown potential in treating inflammatory skin diseases. For instance, extracts from *Hypericum perforatum* L. (Schempp et al., 2003) and *Melissa officinalis* L. (Yargholi et al., 2021) have undergone clinical trials, demonstrating a significant reduction in symptoms of AD and psoriasis. However, their efficacy is limited due to low penetration into the skin and cells, as well as rapid oxidative decomposition in bodily fluids, which prevents the achievement of effective therapeutic levels in target cells. Recently, plant-derived nanovesicles (PDNVs) have emerged as a promising alternative due to their natural bioactivity, and enhanced bioavailability (Jung et al., 2025; Kalarikkal et al., 2025). Moreover, they are produced at high yields and exhibit low immunogenicity (X. Chen et al., 2023).

Extracts of *Melissa officinalis* L., or commonly known as Lemon Balm (LB), were shown to decrease DNA damage in UVB-stressed keratinocytes (Pérez-Sánchez et al., 2016) and significantly inhibit epidermal hyperplasia and scaling in imiquimod (IMQ)-induced psoriasis mice model (Dimitris et al., 2020). Nevertheless, the potential of LB-NVs remains unexplored, and their effect on skin cells and mitochondrial function under inflammatory conditions has not yet been investigated.

In our study, we aimed to investigate the effect of LB-NVs on bioenergetics, mitochondrial dynamics and inflammatory signalling in fibroblasts. We induced a pro-inflammatory state (PInfS) using a cytokine cocktail comprising IL-22, IL-17A, and TNF-α, and assessed the effect of LB-NVs on mitochondrial network integrity and fission (p-Drp1), metabolic shift from mitochondria toward glycolysis, and activation of inflammatory mediators including p38 MAPK, IL-18, IL-4, IL-13 and IL-23.

2. Materials and methods

2.1. Cell cultures and treatments

Human fibroblasts (BJ-5ta, RRID:CVCL_6573, ATCC, Manassas, VA, USA) were cultured in complete medium consisting of DMEM (high glucose, GlutaMAX supplement, Gibco, 10,566,016) supplemented with 10 % fetal bovine serum (Gibco, 26,140,079) and 1 % penicillin/streptomycin (Sigma, P0781) at 37 °C. For the assays, cells were pre-treated with cytokines to induce a pro-inflammatory state, one day after cell seeding. The cytokine mix included TNF-α (5 ng/ml, SRP3177), IL-22 (10 ng/ml, SRP3089), and IL-17 (10 ng/ml, SRP3080) (all from Sigma-Aldrich). After 24 h, NVs were added to the medium at a concentration of 2.1×10^8 NV/1 cm^2 and treated for 48 h. Control cells were treated with Phosphate-Buffered Saline (PBS) (Thermo Fisher Scientific, 18912014, pH=7.45), corresponding to the vehicle used for NVs or cytokine mix treatments. A mitochondrial division inhibitor, Mdivi1 (Sigma, 475,856), was applied at a concentration of 25 μM, 24 h prior to the experiment.

2.2. Isolation of NVs from plants

Dried aerial parts of *Melissa officinalis* L. (Alfred Galke GmbH, Germany), *Scutellaria baicalensis, Hypericum perforatum* L., *chelidonium Majus* L., *Artemisia dracunculus* L. (provided by the Laboratory of Plant Physiology in the Lithuanian research centre for agriculture and forestry) were used for NVs isolation. The isolation was performed using a polymer precipitation method with the ExoPLANT-Lo kit (Exolitus). In short, 4 *g* of dried plant material was mixed with stabilising reagents A and B. The mixture was gently shaken at 30 rpm for 3 h, followed by centrifugation at 1000 × g for 10 min. The resulting supernatant was centrifuged again at 3000 × *g* for 15 min to remove undissolved debris. Afterwards, the supernatant was filtered through a 0.22 μm vacuum filter. The filtrate was combined with reagent C in a 1:1 ratio and incubated at 4–8 °C for 16 h. The mixture was then centrifuged at 3000 × *g* for 1 hour. The supernatant was discarded, and the resulting nanovesicle pellet was resuspended in 400 μl PBS.

2.3. Physical and chemical characterisation of NVs

The physical properties of NVs, including yield and size, were assessed using Nanoparticle Tracking Analysis (NTA), with NanoSight NS300 instrument (Malvern Panalytical, Grovewood Road, Malvern, UK). Samples were diluted 1:3000 in PBS, and five videos of 60 s duration were captured. Data were processed by NTA 3.0 software (Malvern Instruments), which was optimised to initially identify each particle and then monitor its movement across frames. Analysis settings included a camera level of 11 and a detection threshold of 5.

Cryo-electron microscopy (Cryo-EM) was used to visualise vesicles in their native state. Sample grids (Cu300 mesh R1.2/1.3 holey carbon, Quantifoil, X-301-CU300) were first glow-discharged using the GloQube Plus system (Quorum Technologies) for 45 s at 20 mA to enhance sample adherence. Following this, 3 μL of the aqueous vesicle suspension was deposited onto the carbon-coated side of the grid. The grids were then blotted for 5 s and plunge-frozen in liquid ethane using a Vitrobot Mark IV (Thermo Fisher Scientific) at 4 °C. This vitrification process preserved vesicle ultrastructure by embedding them in a thin amorphous ice layer. Imaging was performed using a Glacios cryo-electron microscope (Thermo Fisher Scientific) operating at 200 kV, equipped with a Falcon 3EC Direct Electron Detector in electron counting mode (Vilnius University, Lithuania). Highest resolution images were acquired using EPU software (v2.14.0) at a nominal magnification of 92,000 ×, corresponding to a calibrated pixel size of 1.10 Å/pixel. The exposure time was 46.3 s, with a total dose of 30 $e^-/Å^2$ per image, and −2.0 μm defocus. Lower magnification images we acquired at a nominal magnification of 11,000 × with the exposure time of 10 s and −80.0 μm defocus.

RNA were isolated from LB-NVs samples using PureLink RNA Mini Kit (Invitrogen, Thermo Fisher Scientific, 12183020). To prepare the samples, 100 μL of a 10^8/ml nanovesicle solution was combined with 300 μL of lysis buffer, following the manufacturer's protocol. RNA concentration was determined using a microplate reader (VarioskanTM LUX, Thermo Scientific™, Waltham, Massachusetts, USA) with the μDrop™ and μDrop Duo Plate (Thermo Scientific™) for measurement. The content of RNA was normalised to 1×10^{10} particles.

2.4. Cellular respiration

Cells were seeded in Seahorse XFp cell culture plates at a density of 1700 cells/well and treated as previously described. Bioenergetic

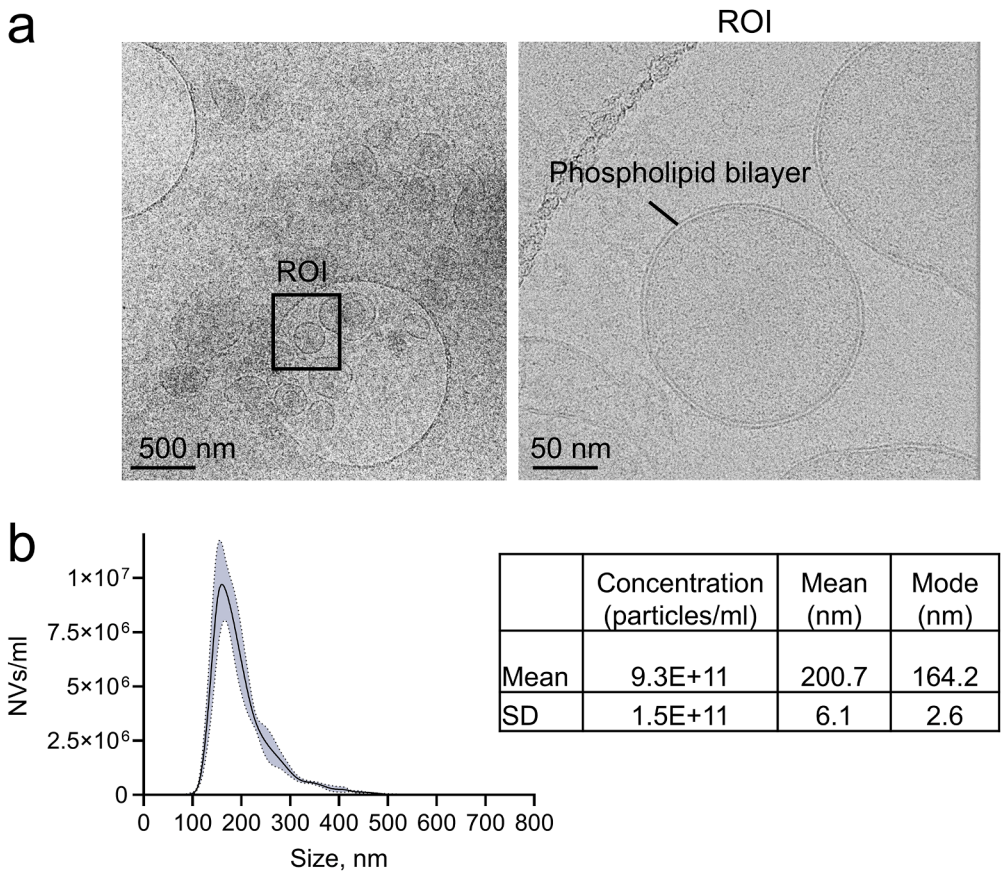

	Concentration (particles/ml)	Mean (nm)	Mode (nm)
Mean	9.3E+11	200.7	164.2
SD	1.5E+11	6.1	2.6

Fig. 1. Characterisation of lemon balm-derived nanovesicles (LB-NVs). (a) Representative Cryo-EM images. (b) Size distribution assessed by nanoparticle tracking analysis on the left panel and a table of physical characteristics of LB-NVs on the right panel. Data: mean with SD, $n = 4$.

function was assessed using Seahorse XFp analyser (Agilent Technologies, Santa Clara, CA, USA), in combination with the XFp MitoStress Test kit, following the manufacturer's protocol. On the day of the experiment, cell media was changed to XF DMEM supplemented with 10 mM glucose, 1 mM pyruvate, 2 mM glutamine and incubated for 1 hour in an incubator without CO_2. Final concentrations of MitoStress Test kit inhibitors were: 1.5 μM oligomycin, 2 μM FCCP, and 0.5 μM rotenone and antimycin A. Seahorse plates (103025–100), test kits (103022–100), media and supplements were purchased from Agilent Technologies. Results were normalised to the number of nuclei, which were counted after analysis using fluorescent microscopy following Hoechst 33342 staining (7 μg/ml, 5 min, Invitrogen, H21492) and expressed as x 10^3 nuclei per well.

2.5. Presto blue assay

Cells were seeded into 96-well plates at a density of 4000 cells per well and treated as previously described. Metabolic activity was evaluated using the PrestoBlue™ Cell Viability Reagent (Invitrogen, A13261) according to the manufacturer's instructions. Briefly, the medium was replaced with a solution containing 10 % PrestoBlue in fresh culture medium, followed by a 1-hour incubation in the dark. Absorbance was measured at 570 nm with a reference at 600 nm using a Varioskan™ LUX microplate reader (Thermo Scientific™, Singapore).

2.6. Mitochondrial morphometry

Cells were seeded at a density of 30,000 per well in glass-bottom four-well chambers (Thermo Scientific™, 155382). Mitochondria were labelled by incubating the cells with 100 nM Mito Live Orange (Abberior, LVORANGE-0146–30NMOL) for 40 min in serum-free medium, followed by three rapid rinses and a further 40 min wash. The staining medium was then replaced with HBSS (Gibco), and imaging was performed using a Zeiss Axio Observer.Z1 fluorescence microscope (Zeiss, Oberkochen, Germany). Mitochondrial morphology was assessed using the MiNA (Mitochondrial Network Analysis) plugin in Fiji (Valente et al., 2017) quantifying parameters such as mitochondrial footprint, network branches mean, summed branch lengths mean. For each experimental group, a minimum of 10 cells was analysed in three independent experiments.

2.7. Mitochondrial ROS analysis

Cells were seeded at a density of 4000 cells per well in 96-well plates and treated as described previously. For Mitochondrial ROS (MitoROS) assessment, cells were incubated with 200 nM MitoTracker™ Red CM-H_2Xros (Invitrogen, M7513) in DMEM supplemented with 1 % penicillin/streptomycin for 30 min. Following incubation, cells were washed once and counterstained with Hoechst 33,342 (7 μg/mL) for 5 min. Cells were then washed twice and imaged in phenol red-free DMEM. Antimycin A (Sigma-Aldrich, A8674), used as a positive control to induce superoxide production, was added during the dye incubation at a final concentration of 50 μM. Fluorescence images were acquired using an Olympus APX100 microscope. Image analysis was performed using Fiji software, applying threshold-based segmentation with the Huang algorithm. MitoROS fluorescence intensity was normalised to cell number, determined by counting Hoechst-positive nuclei. Data were expressed relative to the control group, which was set to 100 %.

2.8. Protein secretion analysis

Protein secretion was assessed using the Human Custom

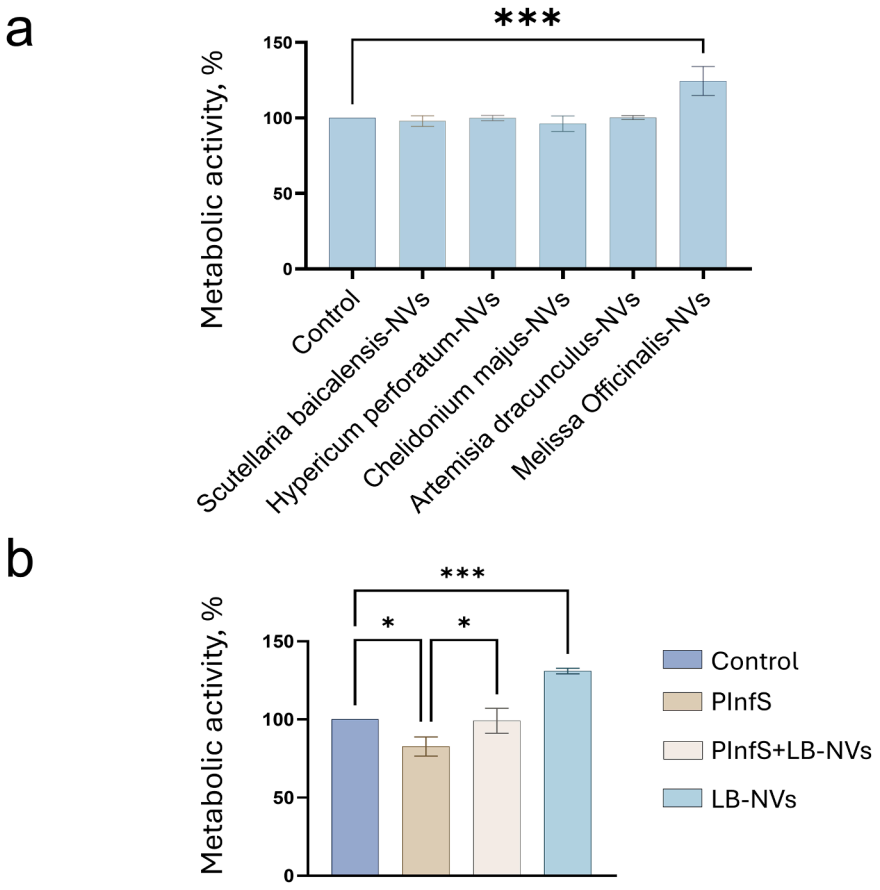

Fig. 2. Plant-derived nanovesicle effect on metabolic activity in fibroblasts. (a) *Scutellaria baicalensis, Hypericum perforatum* L., *Chelidonium majus* L., *Artemisia dracunculus* L., *Melissa officinalis* L. (Lemon balm, LB)-derived NVs' effect on the metabolic activity of fibroblasts. Statistics: One-way ANOVA, Dunnett's test. (b) LB-NVs effect on metabolic activity in pro-inflammatory state (PinfS)-induced fibroblasts. Control – PBS-treated cells. Statistics: One-way ANOVA, Fisher's LSD test. *$p <$ 0.05, *** $p < 0.001$, $n = 3$. Data: mean with SD.

ProcartaPlex kit (PPX-05-MXDJZ2H, Thermo Fisher Scientific) on a Luminex 200 system (Luminex Corp, Austin, TX), following the manufacturer's instructions. Data were collected and analysed using xPONENT software. Protein concentrations (pg/ml) were determined based on standard curves generated for each analyte. Measurements above the upper detection limit were assigned the highest value from the respective standard curve, while values below the detection threshold were recorded as zero.

2.9. Western blot

Cells were seeded at a density of 54,000 per well in a 12-well plate and treated as described previously. Cells were lysed with RIPA buffer (CST, 9806) containing 1x protease inhibitor cocktail (CST, 5871) for 15 min on ice. Lysates were centrifuged at 18.000 x g for 20 min at 4 °C to remove cell debris. Protein concentration was determined with Bradford reagent (Sigma, B6916) and evaluated using Varioskan™ LUX microplate reader. For Western Blot, analysis was performed as described earlier (Kulkovienė et al., 2025). Briefly, protein samples (10 μg/lane) were denatured in 4 × Laemmli buffer with 4 % β-mercaptoethanol at 95 °C for 5 min, separated by SDS–PAGE, and transferred to 0.2 μm nitrocellulose membranes using a wet transfer system. Membranes were blocked in 3 % BSA/TBST for 1 hour at room temperature (RT) and incubated overnight at 4 °C with primary antibodies: phospho-DRP1 (Ser616) (CST, 3455, 1:1000), DRP1 (CST, 8570, 1:1000), p-p38 (SCT, 4511, 1:1000); p38 (CST, 9212, 1:1000), p-NF-κB p65 (CST, 3033, 1:1000), p-NF-κB p65 (CST, 8242, 1:1000) or GAPDH (Invitrogen, MA5–15738, 1:4000). After TBST washes, membranes were incubated with HRP-conjugated goat anti-rabbit (Carl Roth, 4750) or goat anti-mouse (Carl Roth, 4759) secondary antibodies (1:10,000, 1 h, RT). When detecting proteins of similar molecular weight, membranes were stripped using a mild stripping solution (1,5 % glycine, 0,1 % SDS, 1 % Tween-20) for 15 min at RT, washed 3 × with TBST and blocked for 30 min prior to re-probing. Bands were visualized with ECL (Thermo Scientific) and imaged using the Alliance Q9 system; densitometry analysis was performed with NineAlliance™ software.

2.10. Quantification and statistical analysis

All experiments were performed in at least 3 independent biological replicates with ≥2 technical replicates per experiment. Luminex analyses were conducted using 3–5 independent biological replicates; Western Blot analyses used 3 biological replicates without technical replication. Results were expressed as mean ± SD. For group comparisons, we applied one-way ANOVA, Fisher's LSD and Dunnett's tests. Statistical analysis was performed using GraphPad Prism software (GraphPad Software, Inc., USA).

3. Results

3.1. Characterisation of LB-NVs

LB-NVs were characterised by physical and chemical properties, including size distribution by nanoparticle tracking analysis (NTA), morphology by cryo-electron microscopy (Cryo-EM), and RNA concentration. Cryo-EM examination confirmed phospholipid membrane-

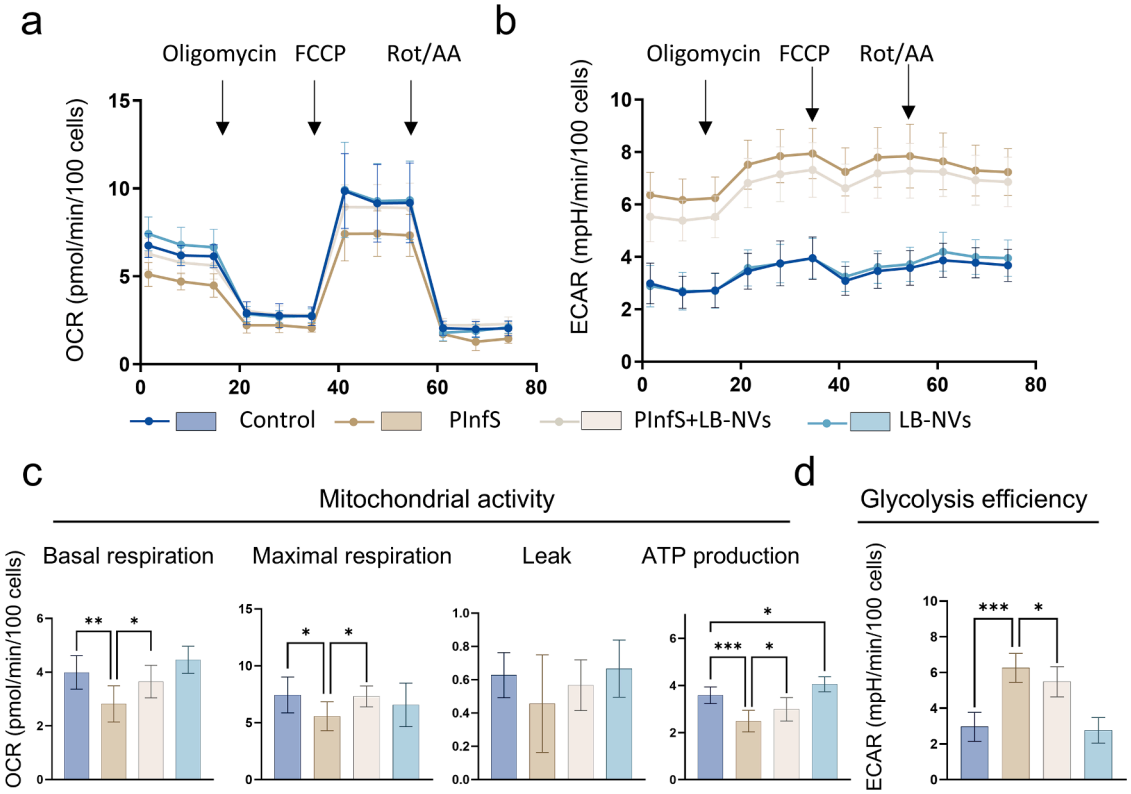

Fig. 3. Lemon balm-derived nanovesicles' (LB-NVs) effect on mitochondrial and glycolysis efficiency in pro-inflammatory state (PInfS)-induced fibroblasts assessed by Seahorse XFp using Mito Stress kit. (a) Mitochondrial oxygen consumption rate (OCR) curves. (b) Extracellular acidification rate (ECAR) curves. Both OCR and ECAR were measured simultaneously. Arrows mark injections of respiration modulators to reveal key parameters of mitochondrial function shown in (c). Basal respiration is measured at three initial points, while maximal respiration is measured after injecting FCCP to uncouple oxidative phosphorylation and ATP synthesis. Proton leak is measured by OCR after Oligomycin (ATPase inhibitor) injection, with ATP synthesis calculated by subtracting proton leak-stimulated respiration from basal. Rotenone and Antimycin A (Rot/AA), which are complex I and III inhibitors, inhibit mitochondrial respiration, enabling calculation of non-mitochondrial respiration, which is subtracted from OCR values. (d) Glycolytic efficiency is calculated from basal ECAR prior to injections. Control – PBS-treated cells. Statistics: One-way ANOVA, Fisher LSD test, *$p < 0.05$, **$p < 0.01$, *** $p < 0.001$, $n = 3$. Data: mean with SD.

enclosed vesicles, with an average size of 185 nm in diameter (Fig. 1a). LB-NVs ranged in size from 100 nm to 300 nm, with a mean size of 200.7 (SD=6.1 nm), while the majority had a size of 164.2 (SD=2.6 nm) (Fig. 1b). Thus, NTA results were largely consistent with those of the cryo-EM images, indicating a general size consistency of the vesicle samples. Additionally, LB-NVs yield from 4 g of dried material were 9.3×10^{11} (SD=1.5×10^{11})particles/ml, and they contain 3.3 μg/10^{10} RNA (0.74 μg/g dry weight). Particle concentration was considered to normalise NVs treatments in all assays.

LB-NVs were evaluated according to their biological effect in fibroblasts. To compare their activity with other PDNVs, NVs were also isolated from phylogenetically related plants (*Scutellaria baicalensis, Hypericum perforatum* L., *Chelidonium majus* L., *Artemisia dracunculus* L.), whose extracts were previously reported to have anti-inflammatory effect in skin inflammation (Dimitris et al., 2020; Jung et al., 2012; Yang et al., 2011; Yücel et al., 2017; Yun et al., 2016). Among all tested preparations, LB-NVs were particularly notable for their impact on metabolic activity, increasing it by 25.4 % compared to PBS-treated controls (Fig. 2a). NVs from *Scutellaria baicalensis, Hypericum perforatum* L., *Chelidonium majus* L., *Artemisia dracunculus* L. had no effect on the metabolic activity of fibroblasts.

In a previous study, we demonstrated that PInfS induced with the same cytokine cocktail (IL-17, IL-22, and TNF-α) reduces metabolic activity in fibroblasts (Kulkovienė et al., 2025). Treatment with LB-NVs reversed this suppression to the basal level (Fig. 2b), revealing an inflammation-protective effect (Fig. 2b).

3.2. LB-NVs normalise bioenergetic processes of fibroblasts under pro-inflammatory conditions

It has been shown that PInfS may reprogram cellular metabolism in fibroblasts by reducing mitochondrial respiration and increasing glycolysis. The observed changes in fibroblasts' metabolic activity following LB-NVs treatment pointed to possible effects on mitochondrial and glycolytic pathways. Consequently, we assessed cellular bioenergetics using the Seahorse XFp analyser.

We observed that PInfS lowered the overall oxygen consumption rate (OCR) by 25–30 % (Fig. 3a) and increased the extracellular acidification rate (ECAR) by 112 % (Fig. 3b) compared to the control. OCR reduction was significantly restored by LB-NVs: basal mitochondrial respiration was reversed by 21 %, maximal respiration by 23 % and ATP production by 14 % compared to the OCR of PInfS-affected fibroblasts in the respective parameters (Fig. 3c). Notably, LB-NVs alone elevated ATP production by 13 % compared to control, indicating enhanced efficiency of the phosphorylating system (Fig. 3c). Additionally, PInfS-induced ECAR elevation was lowered by 26 % with LB-NVs treatment (Fig. 3d).

Overall, these results indicate that LB-NVs restore suppressed mitochondrial respiration and ATP generation, while also attenuating glycolysis stimulation in PInfS-induced fibroblasts, thereby recovering a balanced bioenergetic state associated with inflammation resolution.

3.3. LB-NVs reverse mitochondrial fragmentation induced by the pro-inflammatory state through regulation of Drp-1

Metabolic processes are closely linked to mitochondrial network

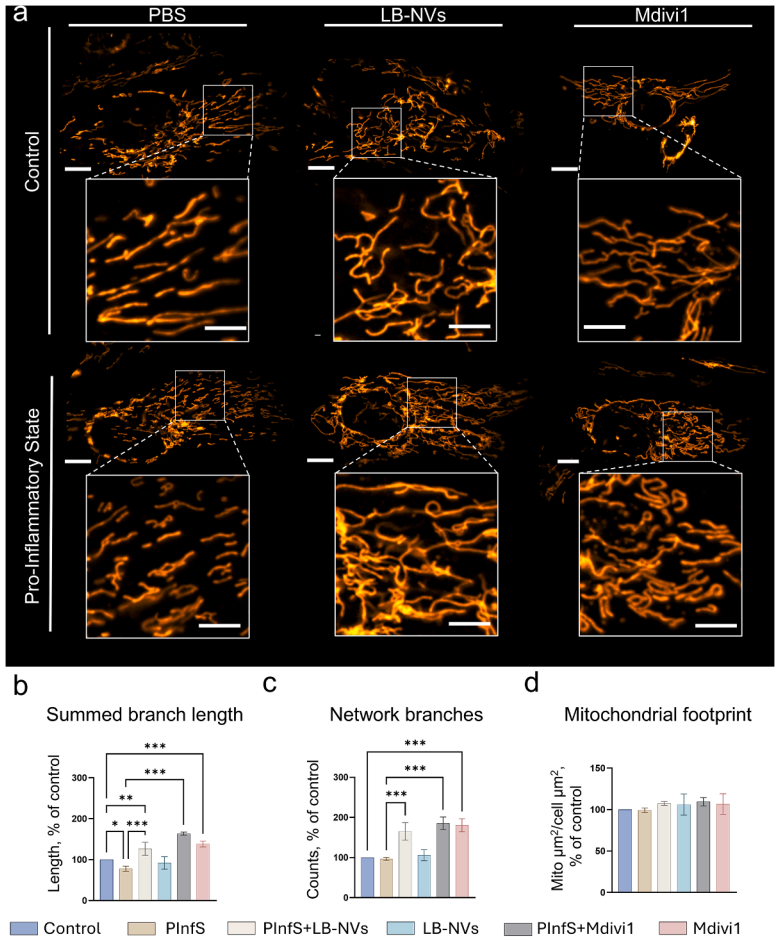

Fig. 4. Effect of lemon balm-derived nanovesicles (LB-NVs) on mitochondrial fragmentation in pro-inflammatory state (PInfS)-induced fibroblasts. Mdivi1 – Mitochondrial fission inhibitor, used as a positive control. (a) Representative images of the mitochondrial network. Scale for full cell mitochondrial network – 10 µm, scale for ROI – 5 µm. (b) Quantitative results of mitochondrial network parameters calculated by MiNa morphology analysis tool in ImageJ. These parameters include combined lengths of branches per individual structure, the mean number of network branches and mitochondrial footprint normalised to cell area. Control – PBS-treated cells. Statistics: One-way ANOVA, Fisher LSD test, $*p < 0.05$, $*** p < 0.001$, $n = 3$. Data: mean with SD.

integrity, as reduced mitochondrial respiration is often associated with fragmented mitochondria (W. Chen et al., 2023). Previous results showed that the same cytokine cocktail can induce mitochondrial fission in fibroblasts. To examine what effect LB-NVs have on fragmented networks, we performed mitochondrial morphometry analysis as described in (Kulkovienė et al., 2025). As a positive control to reverse PInfS-induced fragmentation, we used Mdivi1. It inhibits mitochondrial fission through suppressing dynamin-related protein 1 (Drp1), which is a GTPase responsible for mediating mitochondrial division.

Representative images (Fig. 4a) show that under PInfS, mitochondria appear shorter and sparsely distributed. Co-treatment with LB-NVs markedly restored mitochondrial interconnectivity, not only reaching the control-like morphology but even enhancing network complexity.

Morphology analysis using the MiNa plugin in ImageJ confirmed these observations. Summed branch length, which reflects the overall extent of mitochondrial elongation, was reduced by PInfS by 22 % (Fig. 4b). This was not only restored by LB-NVs but also increased by 27 % compared to the control. A similar effect was observed with Mdivi1, which increased summed branch length by 38 % compared to the control and by 63 % in the presence of PInfS. Furthermore, LB-NVs increased the number of network branches, which indicates a degree of connectivity, by 65 % in PInfS-induced cells. A similar effect was observed with Mdivi1, which increased the number of network branches by 80 % compared to the control and by 85 % in the presence of PInfS (Fig. 4c). Interestingly, LB-NVs alone did not induce any changes, indicating that they act only under inflammatory conditions, unlike Mdivi1. Mitochondrial area remained unchanged in all experimental groups (Fig. 4d).

Overall, these results demonstrate that LB-NVs can reduce the fragmentation induced by PinfS in fibroblasts. Moreover, the similar effect of LB-NVs and Mdivi1 raises the possibility that LB-NVs may preserve mitochondrial network integrity through a mechanism similar to Mdivi1, potentially involving Drp1 regulation.

Drp1 is activated by a post-translational modification, usually phosphorylation of Ser616. To examine whether LB-NVs influence the activation of Drp1, we performed Western Blot analysis.

Western blot analysis revealed that phosphorylation of Drp1 at Ser616 (p-Drp1) tended to be elevated under PInfS, showing a 12 % increase relative to control (Fig. 5a and b). Treatment with LB-NVs reversed this trend, reducing p-Drp1 levels by 30 %, suggesting that they suppress Drp1 phosphorylation and thereby limit mitochondrial fission (Fig. 5a and b).

3.4. LB-NVs selectively reduce total p38 MAPK levels under pro-inflammatory conditions

Drp1 activation is often associated with increased MitoROS production, which in turn can contribute to the activation of NF-κB and p38 MAPK signalling pathways.

To test whether LB-NVs may alleviate PinfS-induced MitoROS

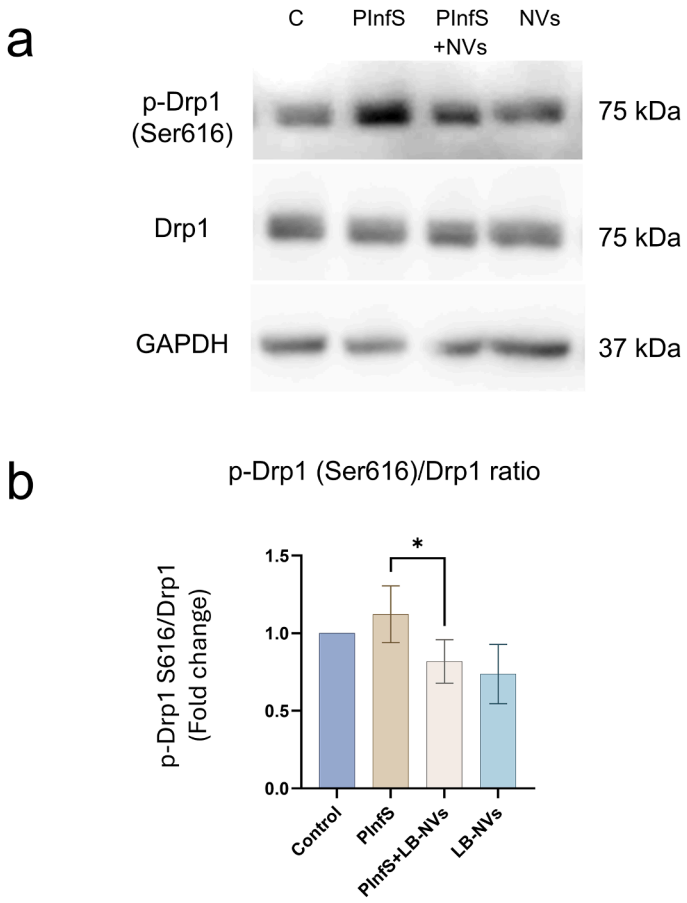

Fig. 5. Effect of lemon balm-derived nanovesicles (LB-NVs) on dynamin-related protein 1 (Drp1) activation in pro-inflammatory state (PinfS)-induced fibroblasts. (a) Western blots showing protein levels of phosphorylated (Ser616)-Drp1 and total Drp1. C-control. (b) Densitometric analysis of pDrp (Ser616)/total Drp1 ratio, normalised to loading control GAPDH. Data: mean withSD. Control – PBS-treated cells. Statistics: One-way ANOVA, Fisher's LSD test. $n = 3$. *$p < 0.05$.

increase, we used a reduced MitoTracker CM-H2Xros probe. Additionally, Antimycin A, a superoxide inducer, was used as a positive control, and MitoTempo, a superoxide scavenger, as a negative control (Fig. 6a).

PInfS induced a strong increase in MitoROS (159 % vs. control). While LB-NV co-treatment showed a trend toward reduced MitoROS levels (135.5 % of control), this effect did not reach statistical significance (Fig. 6b).

To assess the impact of MitoROS on inflammatory signalling, we measured both total and phosphorylated p38 MAPK and NF-κB p65, key mediators of cytokine-driven inflammation. Western blot analysis demonstrated that LB-NVs significantly reduced total p38 MAPK protein content in fibroblasts exposed to pro-inflammatory conditions, with a 60 % decrease compared to PInfS-treated cells and a 45 % decrease relative to control (Fig. 7a and c). In contrast, LB-NVs did not significantly alter the levels of phosphorylated p38 (p-p38). Consequently, the p-p38/p38 ratio was increased fivefold in PInfS-treated fibroblasts and further elevated to 7.5-fold upon LB-NV treatment. Importantly, this increase in the p-p38/p38 ratio reflects a reduction in total p38 content rather than an increase in p38 phosphorylation (Fig. 7a and c). NF-κB signalling analysis revealed an 8.3-fold and 7.2-fold increase in the p-p65 and p-p65/p65 ratio under PInfS conditions, respectively; however, LB-NV treatment did not significantly affect either the p-p65/p65 ratio or total p65 protein levels (Fig. 7b and d).

These results indicate that LB-NVs treatment does not significantly suppress MitoROS or canonical NF-κB, p38 MAPK activation. Instead, LB-NVs reduce total p38 MAPK level without altering its phosphorylation.

3.5. LB-NVs impact cytokine secretion

To evaluate whether mitochondrial function restoration by LB-NVs is accompanied by changes in the secretion of cytokines, their levels were measured in fibroblast media. IL-4, IL-13, IL-18, and IL-23 were selected for this analysis based on preliminary screening with the 20-plex Human Inflammation panel (data not shown), which identified cytokines modulated by LB-NVs. For comparison, we also analysed the effects of Mdivi1 to determine whether modulation of mitochondrial dynamics correlated with changes in cytokine secretion.

LB-NVs selectively reduced cytokine secretion in fibroblasts exposed to PInfS. IL-4 levels increased from 1.5 pg/ml in untreated cells to 267.0 pg/ml under PInfS and were reduced by 26 pg/ml following LB-NVs treatment, corresponding to a 10 % decrease (Fig. 8a). IL-13 was undetectable under control conditions and increased significantly under PInfS up to 1.9 pg/ml. LB-NVs treatment reduced IL-13 levels by 0.9 pg/ml, representing an almost 50 % decrease. (Fig. 8b). IL-18 (undetectable in control conditions) reached 17.1 pg/ml under PInfS and LB-NVs significantly reduced it by 13.1 pg/ml, corresponding to a 76 % reduction (Fig. 8c). These changes indicate that LB-NVs suppressed secretion of cytokines associated with general inflammation (IL-18) and with T helper (Th) type 2 cell-driven pathways (IL-4, IL-13), which are central to atopic dermatitis. In contrast, IL-23, linked to Th17 responses and psoriasis-associated inflammation, was not affected (Fig. 8d). Notably, Mdivi1 exhibited a broader anti-inflammatory effect, decreasing IL-4, IL-13, and IL-18 by 30 %, 81 %, and 91 %, respectively, and also lowering IL-23 by 60 % compared to PInfS conditions.

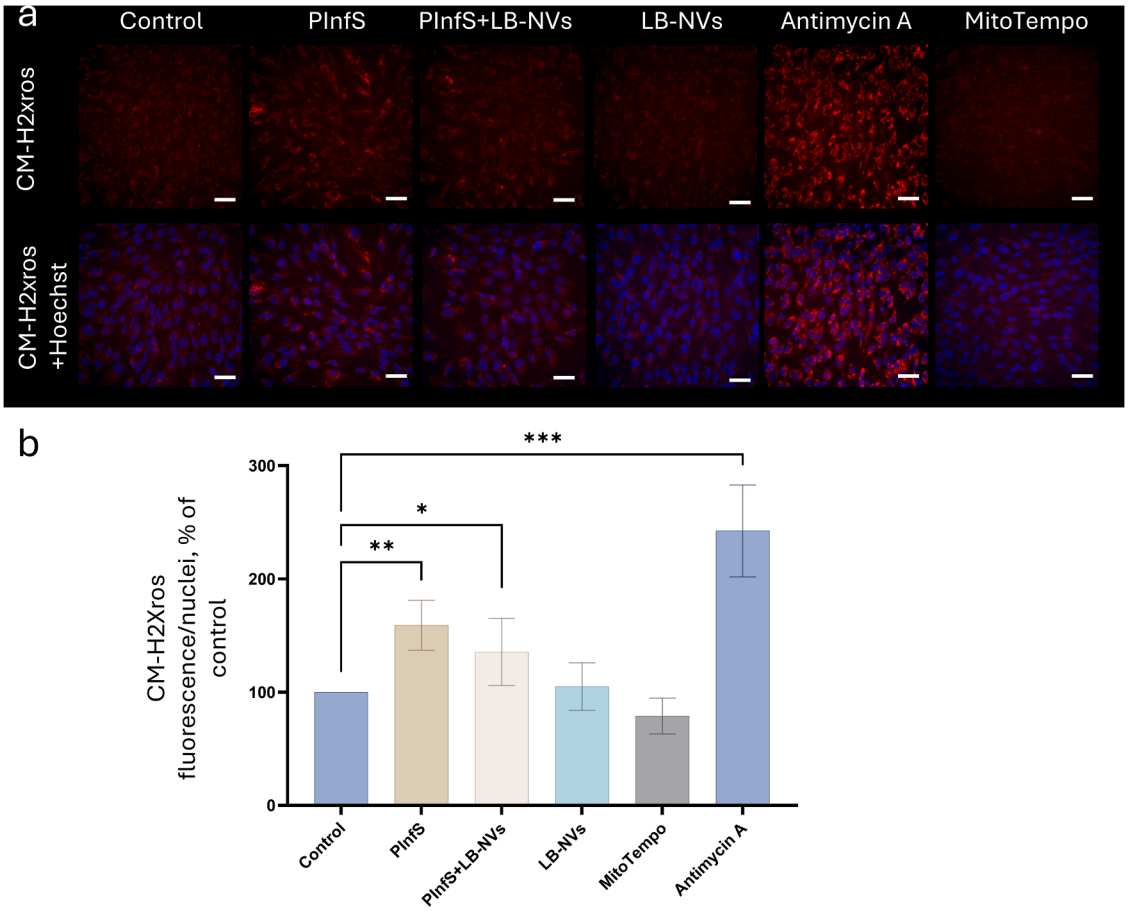

Fig. 6. Effect of lemon balm-derived nanovesicles (LB-NVs) on mitochondrial ROS production in pro-inflammatory state (PInfS)-induced fibroblasts. (a) Representative images of cells labelled with reduced MitoTracker CM-H2xros, indicating MitoROS. Antimycin A was used as a positive control for increased ROS production and MitoTempo, a mitochondrial superoxide scavenger, served as a negative control. Scale bar – 50 μm. (b) Quantitative results of CM-H2xros fluorescence intensity normalised to nuclei number, determined by Hoechst 33,342 staining. Control – PBS-treated cells. Statistics: One-way ANOVA, Fisher LSD test, $^{*}p < 0.05$, $^{**}p < 0.01$, $^{***}p < 0.001$, $n = 3$–4. Data: mean with SD.

4. Discussion

In our study, we showed that LB-NVs can (i) normalise bioenergetic processes in fibroblasts by restoring suppressed mitochondrial respiration and reducing the elevated glycolysis efficiency under PInfS; (ii) reverse mitochondrial fragmentation in PInfS-induced fibroblasts by suppressing the Drp1 phosphorylation at Ser616 and thereby preventing its activation; (iii) reduce total p38 MAPK protein level, without changing its phosphorylation state and (iv) lower PInfS-induced secretion of IL-4, IL-13 and IL-18. To our knowledge, this is the first study to demonstrate the protective effect of LB-NVs on skin cells under inflammatory conditions, restoring cellular energy metabolism and the mitochondrial network, and blocking the release of inflammatory mediators.

Mitochondrial dysfunction, including impaired ATP production, can significantly contribute to skin inflammation, and restoring mitochondrial function offers new strategies for the treatment of skin diseases (Ahmad Jamil and Abdul Karim, 2025). Fibroblasts are particularly susceptible to mitochondrial dysfunction and play a significant role in inflammatory responses. In our study, LB-NVs restored basal and maximal mitochondrial respiration, and, most importantly, ATP production in fibroblasts during inflammation. These effects were associated with changes in mitochondrial network dynamics.

In inflammatory diseases, fibroblasts acquire an activated phenotype characterised by enhanced aerobic glycolysis and reduced oxidative phosphorylation (OXPHOS). This metabolic shift contributes to the inflammatory microenvironment by promoting the secretion of pro-inflammatory cytokines (Farah et al., 2021). Our results demonstrated that LB-NVs promote metabolic reprogramming by normalising suppressed OXPHOS and reducing glycolytic efficiency in PInfS-induced fibroblasts. Similarly, garlic-derived NVs demonstrated metabolic reprogramming in LPS-affected human gingival fibroblasts and reduced inflammation by activating phosphoglycerate dehydrogenase (PHGDH), a crucial regulator of mitochondrial function (Yu et al., 2025). Moreover, carrot-derived NVs were able to reduce bone loss in osteoporotic mice due to their ability to restore mitochondrial functionality. Similar to LB-NVs, carrot-NVs reversed the H_2O_2-inhibited mitochondrial respiration in preosteoblasts. Authors also noticed changes in mitochondrial morphology with carrot-derived NVs treatment: they were able to reduce H_2O_2-caused mitochondrial shrinkage (Peng et al., 2025).

Preserving mitochondrial network integrity is crucial for maintaining efficient mitochondrial function and resolving inflammation. This was demonstrated in a study on *Artemisia annua*-derived NVs, which restored LPS-induced OXPHOS reduction in mouse alveolar macrophages by regulating mitochondrial integrity, as evidenced by longer shape and organised cristae. Restoring mitochondrial functionality also contributed to a decrease in pro-inflammatory cytokine production and ameliorated lung pathology in endotoxin-induced lung injury in mice (Ye et al., 2024). Our study demonstrated that LB-NVs inhibited PInfS-induced mitochondrial fragmentation, evident by increased mitochondrial elongation. They also improved the level of mitochondrial branching, which is important for the rapid and efficient

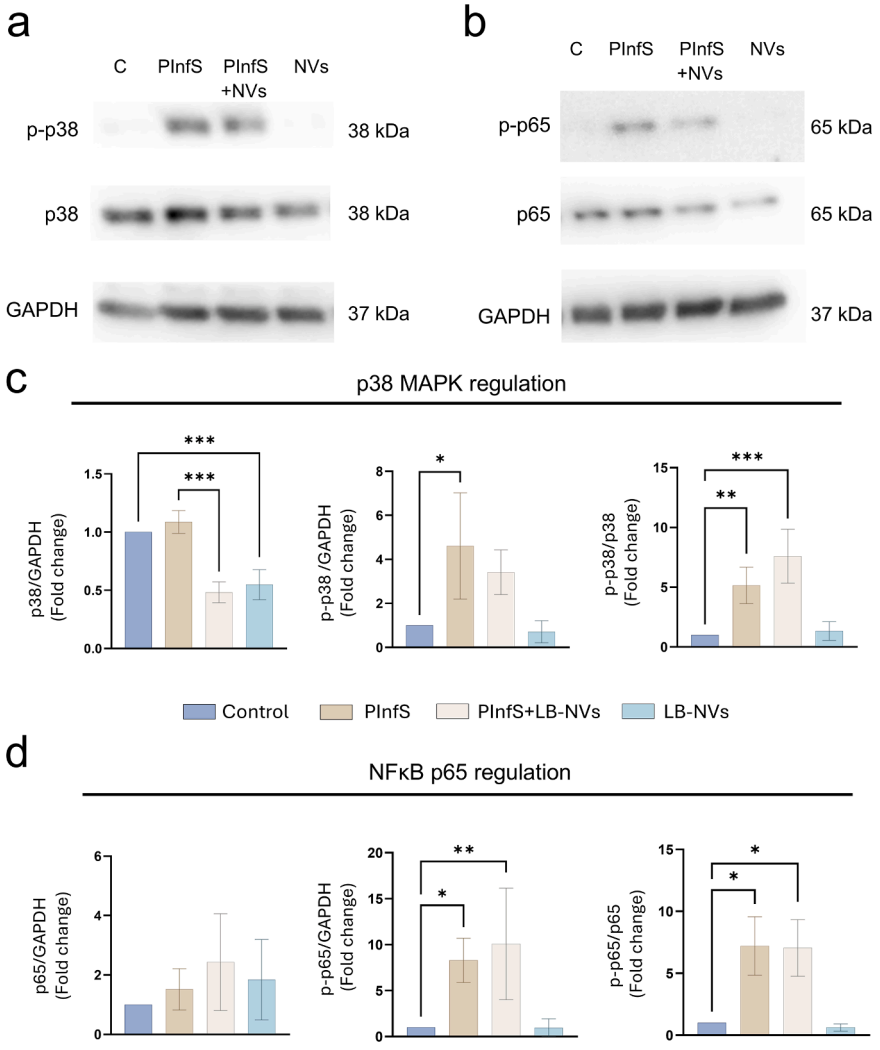

Fig. 7. Effect of lemon balm-derived nanovesicles (LB-NVs) on p38 MAPK and p65 NF-κB activation in pro-inflammatory state (PinfS)-induced fibroblasts. Western blots showing levels of phosphorylated (p-) and total levels of (a) p38 and (b) p65. Densitometric analysis of phosphorylated and total protein levels normalised to the loading control GAPDH (c) and (d). Control - PBS-treated cells. Statistics: One-way ANOVA, Fisher LSD test, $*p < 0.05$, $** p < 0.01$, $*** p < 0.001$, $n = 3$. Data: mean with SD.

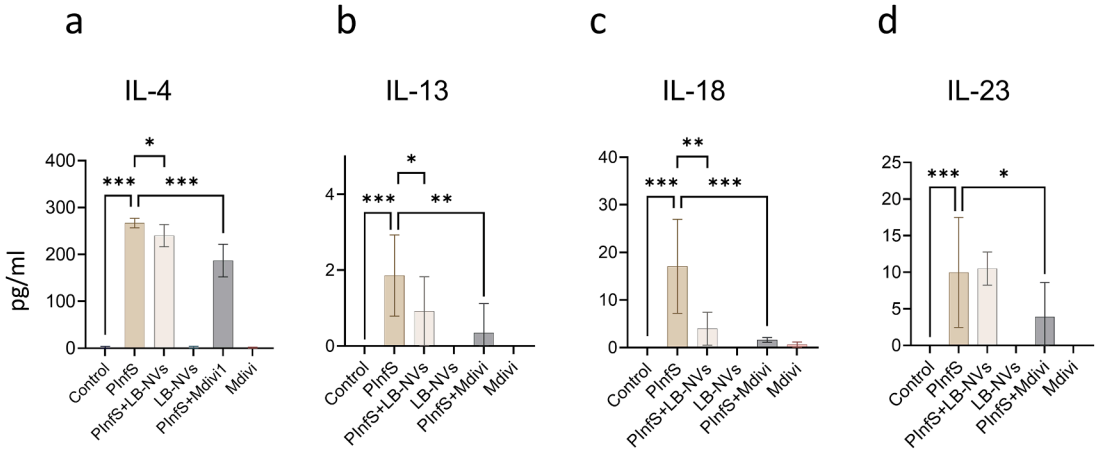

Fig. 8. Lemon balm-derived nanovesicle (LB-NVs) impact on IL-4, IL-13, IL-18 and IL-23 secretion in pro-inflammatory state (PInfS)-induced fibroblasts. Secretion of (a) IL-4, (b) IL-13, (c) IL-18, (d) IL-23. Protein levels were quantified using Luminex xMAP multiplex assay. Control – PBS-treated cells. Statistics: One-way ANOVA, Fisher LSD test, $*p < 0.05$, $**p < 0.01$, $*** p < 0.001$, $n = 5$ (IL-4, IL-13, IL-23); $n = 3$ (IL-18). Data: mean with SD.

distribution of components across the network, maintaining bioenergetic efficiency (Chuphal et al., 2024).

Our results showed that LB-NVs reverse mitochondrial fragmentation by reducing p-Drp1 levels. Similarly, neutrophil-membrane–engineered *Panax ginseng* root NVs were shown to reduce p-Drp1 in LPS-injured mouse lungs and lung epithelial cells. This was followed by significantly restored mitochondrial respiration, inner membrane potential, morphology and improvement of acute lung injury via NLRP3 inflammasome (Ma et al., 2024). Furthermore, a previous study reported that shallot and garlic-derived NVs led to complete skin recovery in the IMQ-induced psoriasis mouse model. These PDNVs were shown to suppress IL-17 via the upstream antioxidant defence system - NRF2 pathway (Kalarikkal et al., 2025). NRF2 activity is closely linked to mitochondrial dynamics (Sabouny et al., 2017; Yan et al., 2022).

Mitochondrial fragmentation via Drp1 activation is closely linked to MitoROS increase (Ahmad Jamil and Abdul Karim, 2025). In the present study, however, LB-NVs did not significantly alter MitoROS levels nor affect the activation status of p38 MAPK or NF-κB, both of which are commonly implicated in ROS-related stress signalling. Consistent with our previous findings, scavenging MitoROS using MitoTempo in fibroblasts did not restore mitochondrial network integrity or reduce inflammation-induced cytokine secretion, whereas mitochondrial fission inhibition with Mdivi1 attenuated the inflammatory response (Kulkovienė et al., 2025). Thus, these data support the concept that, in fibroblasts, modulation of mitochondrial network rather than direct ROS suppression is a key mechanism underlying the anti-inflammatory effects of LB-NVs.

Notably, LB-NVs significantly reduced the total p38 MAPK protein level, without affecting its phosphorylation status. This pattern suggests that LB-NVs attenuate chronic p38-driven inflammatory signalling while preserving acute stress-response capacity. In contrast, NF-κB p65 activation remained unchanged, indicating that essential homeostatic and survival pathways are maintained. Together, these effects suggest that LB-NVs could reduce pro-inflammatory cytokine production and fibroblast hyperactivation in skin inflammation without compromising protective NF-κB–dependent functions, highlighting their potential as a targeted anti-inflammatory intervention.

Furthermore, our results showed that the ability of LB-NVs to reduce PinfS-induced cytokine secretion might be linked to their ability to reverse fragmentation, as Mdivi1 produced similar effects on both mitochondrial dynamics and inflammatory profiles. It was shown that Drp1 inhibition significantly suppressed IL-4 and IL-13 in a 2,4-dinitrochlorobenzene (DNCB)-induced AD mouse model, a finding also evident in our experimental setup (Li et al., 2021). In addition to that, suppressing Drp1 results in p38 MAPK signalling inhibition (Zhang et al., 2015). In line with this, LB-NV treatment significantly reduced total p38 MAPK level, which likely contributes to the observed decrease in IL-4, IL-13, and IL-18 secretion (Jiménez-Garcia et al., 2015; Petrova et al., 2020; Wang et al., 2024).

PDVNs, generally larger than their mammalian counterparts, may reflect differences in biogenesis and cargo requirements, as plants package not only RNAs and proteins but also secondary metabolites and polysaccharides (Karabay et al., 2025; Sall and Flaviu, 2023). Their relatively high miRNA content has been linked to cross-kingdom regulatory effects, including suppression of inflammatory mediators. The vesicle size may thus be functionally advantageous, providing sufficient volume for the delivery of multimodal cargo. LB-NVs used in our study had a mean diameter of 200.7 nm, which is comparable to NVs derived from dried *Vinca minor* (380 nm), *Viscum album* (280 nm) (Woith and Melzig, 2019) and tomato-leaf (201–227 nm) (Viršilė et al., 2024). We quantified total RNA in LB-NVs as part of the chemical NVs characterisation and validation of functionally relevant cargo. The RNA content of LB-NVs (0.74 μg/g dry weight) was comparable to that of dried tomato-leaf NVs, which varied from 0.6 to 3.23 μg/g dry weight (Viršilė et al., 2024). Overall, PDNV characteristics, encompassing both size and RNA content, are species-specific; however, the properties of our LB-NVs closely align with those reported in the literature.

In conclusion, our findings demonstrate that LB-NVs support mitochondrial function and reduce inflammation-driven cytokine secretion in skin fibroblasts. These results highlight LB-NVs as a promising therapeutic approach for inflammatory skin diseases. Further investigation of LB-NVs and their effects on mitochondrial alterations may pave the way for novel treatments for chronic inflammatory conditions.

Data availability statement

No datasets were generated or analysed during the current study. Any additional information required to reanalyse the data reported in this work paper is available from the lead contact upon request.

CRediT authorship contribution statement

Gabrielė Kulkovienė: Writing – review & editing, Writing – original draft, Visualization, Methodology, Investigation, Formal analysis. **Martyna Uldukytė:** Investigation, Formal analysis. **Sofiya Haluts:** Investigation, Formal analysis. **Emilija Mikalauskienė:** Investigation. **Monika Iešmantaitė:** Investigation, Formal analysis. **Giedrė Tamulaitienė:** Investigation. **Giedrius Sasnauskas:** Investigation. **Ramunė Morkūnienė:** Writing – review & editing, Visualization, Supervision, Resources, Project administration, Funding acquisition, Conceptualization. **Aistė Jekabsone:** Writing – review & editing, Supervision, Resources, Project administration, Funding acquisition, Conceptualization.

Declaration of competing interest

The authors declare the following financial interests/personal relationships which may be considered as potential competing interests:

G.K., M.U., A.J., S.H., E.M., and R.M. are co-inventors of a related patent EP25208862, Method for obtaining plant cell vesicles and their compositions with enhanced activity for prevention and treatment of skin inflammation; Priority date: 15/10/2025; Status: pending.

Acknowledgements

This work was supported by the Research Fund of the Lithuanian University of Health Sciences. This project has received funding from the Research Council of Lithuania (LMTLT), agreement No: S-A-UEI-23–7.

Supplementary materials

Supplementary material associated with this article can be found, in the online version, at doi:10.1016/j.ejps.2026.107483.

Data availability

Data will be made available on request.

References

Ahmad Jamil, H., Abdul Karim, N., 2025. Mitochondrial homeostasis: exploring their impact on skin disease pathogenesis. Biomed. Pharmacother. Biomedecine Pharmacother. 189, 118349. https://doi.org/10.1016/j.biopha.2025.118349.

Alalaiwe, A., Chen, C.-Y., Chang, Z.-Y., Sung, J.-T., Chuang, S.-Y., Fang, J.-Y., 2021. Psoriasiform inflammation is associated with mitochondrial fission/GDAP1L1 signaling in macrophages. Int. J. Mol. Sci. 22, 10410. https://doi.org/10.3390/ijms221910410.

Chen, W., Zhao, H., Li, Y., 2023a. Mitochondrial dynamics in health and disease: mechanisms and potential targets. Signal. Transduct. Target. Ther. 8, 333. https://doi.org/10.1038/s41392-023-01547-9.

Chen, X., Wu, Y., Jia, S., Zhao, M., 2024. Fibroblast: a novel target for autoimmune and inflammatory skin diseases therapeutics. Clin. Rev. Allergy Immunol. 66, 274–293. https://doi.org/10.1007/s12016-024-08997-1.

Chen, X., Xing, X., Lin, S., Huang, L., He, L., Zou, Y., Zhang, X., Su, B., Lu, Y., Zheng, D., 2023b. Plant-derived nanovesicles: harnessing nature's power for tissue protection and repair. J. Nanobiotechnol. 21, 445. https://doi.org/10.1186/s12951-023-02193-7.

Chuphal, P., Lanctôt, J.D., Cornelius, S.P., Brown, A.I., 2024. Mitochondrial network branching enables rapid protein spread with slower mitochondrial dynamics. PRX Life 2, 043005. https://doi.org/10.1103/PRXLife.2.043005.

Dimitris, D., Ekaterina-Michaela, T., Christina, K., Ioannis, S., Ioanna, S.K., Aggeliki, L., Sophia, H., Michael, R., Helen, S., 2020. *Melissa officinalis* ssp. *altissima* extracts: a therapeutic approach targeting psoriasis in mice. J. Ethnopharmacol. 246, 112208. https://doi.org/10.1016/j.jep.2019.112208.

Farah, H., Young, S.P., Mauro, C., Jones, S.W., 2021. Metabolic dysfunction and inflammatory disease: the role of stromal fibroblasts. FEBS. J. 288, 5555–5568. https://doi.org/10.1111/febs.15644.

Greb, J.E., Goldminz, A.M., Elder, J.T., Lebwohl, M.G., Gladman, D.D., Wu, J.J., Mehta, N.N., Finlay, A.Y., Gottlieb, A.B., 2016. Psoriasis. Nat. Rev. Dis. Primer 2, 16082. https://doi.org/10.1038/nrdp.2016.82.

Guttman-Yassky, E., Krueger, J.G., 2017. Atopic dermatitis and psoriasis: two different immune diseases or one spectrum? Curr. Opin. Immunol. 48, 68–73. https://doi.org/10.1016/j.coi.2017.08.008.

Jeskey, J., Kurien, C., Blunk, H., Sehmi, K., Areti, S., Nguyen, D., Hostoffer, R., 2024. Atopic dermatitis: a review of diagnosis and treatment. J. Pediatr. Pharmacol. Ther. JPPT 29, 587–603. https://doi.org/10.5863/1551-6776-29.6.587.

Jiménez-Garcia, L., Herránz, S., Luque, A., Hortelano, S., 2015. Critical role of p38 MAPK in IL-4-induced alternative activation of peritoneal macrophages. Eur. J. Immunol. 45, 273–286. https://doi.org/10.1002/eji.201444806.

Jung, D., Kim, N.-E., Kim, S., Bae, J.-H., Jung, I.-Y., Doh, K.-W., Lee, B., Kim, D.-K., Cho, Y.-E., Baek, M.-C., 2025. Plant-derived nanovesicles and therapeutic application. Pharmacol. Ther. 269, 108832. https://doi.org/10.1016/j.pharmthera.2025.108832.

Jung, H.-S., Kim, M.H., Gwak, N.-G., Im, Y.-S., Lee, K.-Y., Sohn, Y., Choi, H., Yang, W.M., 2012. Antiallergic effects of *Scutellaria baicalensis* on inflammation in vivo and in vitro. J. Ethnopharmacol. 141, 345–349. https://doi.org/10.1016/j.jep.2012.02.044.

Kalarikkal, S.P., Kumar, M.N., Rajendran, S., Bethi, C.M.S., Ravilla, J., Narayanan, J., Sundaram, G.M., 2025. Natural plant-derived nanovesicles for effective psoriasis therapy via dual modulation of IL-17 and NRF2 pathway. iScience 28, 112556. doi:10.1016/j.isci.2025.112556.

Karabay, A.Z., Barar, J., Hekmatshoar, Y., Rahbar Saadat, Y., 2025. Multifaceted therapeutic potential of plant-derived exosomes: immunomodulation, anticancer, anti-aging, anti-melanogenesis, detoxification, and drug delivery. Biomolecules. 15, 394. https://doi.org/10.3390/biom15030394.

Kulkovienė, G., Uldukytė, M., Haluts, S., Kairytė, M., Šoliūnas, J., Šalčiūtė, V., Inčiūraitė, R., Skiecevičienė, J., Iešmantaitė, M., Morkūnienė, R., Jekabsone, A.. Psoriasis-like inflammation induces structural and functional changes in mitochondria. doi:10.1101/2024.09.05.611357.

Li, L., Mu, Z., Liu, P., Wang, Y., Yang, F., Han, X., 2021. Mdivi-1 alleviates atopic dermatitis through the inhibition of NLRP3 inflammasome. Exp. Dermatol. 30, 1734–1744. https://doi.org/10.1111/exd.14412.

Ma, C., Liu, K., Wang, F., Fei, X., Niu, C., Li, T., Liu, L., 2024. Neutrophil membrane-engineered Panax ginseng root-derived exosomes loaded miRNA 182-5p targets NOX4/Drp-1/NLRP3 signal pathway to alleviate acute lung injury in sepsis: experimental studies. Int. J. Surg. 110, 72. https://doi.org/10.1097/JS9.0000000000000789.

Peng, J., Liu, R., Xu, J., Yao, Y., Li, B., Chen, D., Chang, Z., Zhao, R., Feng, Y., Hou, R., Lee, M., Zhang, X., 2025. Acid-responsive aggregated carrot-derived nanoantioxidants alleviate oxidative stress and restore osteoblast activity. J. Nanobiotechnol. 23, 206. https://doi.org/10.1186/s12951-025-03235-y.

Pérez-Sánchez, A., Barrajón-Catalán, E., Herranz-López, M., Castillo, J., Micol, V., 2016. Lemon balm extract (Melissa officinalis, L.) promotes melanogenesis and prevents UVB-induced oxidative stress and DNA damage in a skin cell model. J. Dermatol. Sci. 84, 169–177. https://doi.org/10.1016/j.jdermsci.2016.08.004.

Petrova, T., Pesic, J., Pardali, K., Gaestel, M., Arthur, J.S.C., 2020. p38 MAPK signalling regulates cytokine production in IL-33 stimulated Type 2 Innate Lymphoid cells. Sci. Rep. 10, 3479. https://doi.org/10.1038/s41598-020-60089-0.

Sabouny, R., Fraunberger, E., Geoffrion, M., Ng, A.C.-H., Baird, S.D., Screaton, R.A., Milne, R., McBride, H.M., Shutt, T.E., 2017. The Keap1-Nrf2 stress response pathway promotes mitochondrial hyperfusion through degradation of the mitochondrial fission protein Drp1. Antioxid. Redox. Signal. 27, 1447–1459. https://doi.org/10.1089/ars.2016.6855.

Sall, I.M., Flaviu, T.A., 2023. Plant and mammalian-derived extracellular vesicles: a new therapeutic approach for the future. Front. Bioeng. Biotechnol. 11, 1215650. https://doi.org/10.3389/fbioe.2023.1215650.

Schempp, C.M., Hezel, S., Simon, J.C., 2003. Topical treatment of atopic dermatitis with Hypericum cream. A randomised, placebo-controlled, double-blind half-side comparison study]. Hautarzt Z. Dermatol. Venerol. Verwandte Geb. 54, 248–253. https://doi.org/10.1007/s00105-002-0440-y.

Tampa, M., Neagu, M., Caruntu, C., Constantin, C., Georgescu, S.R., 2022. Skin inflammation—a cornerstone in dermatological conditions. J. Pers. Med. 12, 1370. https://doi.org/10.3390/jpm12091370.

Valente, A.J., Maddalena, L.A., Robb, E.L., Moradi, F., Stuart, J.A., 2017. A simple ImageJ macro tool for analyzing mitochondrial network morphology in mammalian cell culture. Acta Histochem. 119, 315–326. https://doi.org/10.1016/j.acthis.2017.03.001.

Viršilė, A., Samuolienė, G., Laužikė, K., Mikalauskienė, E., Balion, Z., Jekabsone, A., 2024. The impact of genotype and controlled environment cultivation parameters on tomato-leaf-derived exosome-like nanoparticle yield and properties. Horticulturae 10, 477. https://doi.org/10.3390/horticulturae10050477.

Wang, J., Liu, Yongjian, Guo, Y., Liu, C., Yang, Y., Fan, X., Yang, H., Liu, Yonggang, Ma, T., 2024. Function and inhibition of P38 MAP kinase signaling: targeting multiple inflammation diseases. Biochem. Pharmacol. 220, 115973. https://doi.org/10.1016/j.bcp.2023.115973.

Weng, Z., Zhou, X., Wu, H., Geng, Y., Zhu, X., Xu, X., Li, J., 2020. Dynamin-related protein 1 expression correlates with psoriasis disease severity and regulates keratinocyte function. Eur. J. Dermatol. 30, 329–337. https://doi.org/10.1684/ejd.2020.3849.

Woith, E., Melzig, M.F., 2019. Extracellular vesicles from fresh and dried plants—simultaneous purification and visualization using gel electrophoresis. Int. J. Mol. Sci. 20, 357. https://doi.org/10.3390/ijms20020357.

Yan, X., Shen, Z., Yu, D., Zhao, C., Zou, H., Ma, B., Dong, W., Chen, W., Huang, D., Yu, Z., 2022. Nrf2 contributes to the benefits of exercise interventions on age-related skeletal muscle disorder via regulating Drp1 stability and mitochondrial fission. Free Radic. Biol. Med. 178, 59–75. https://doi.org/10.1016/j.freeradbiomed.2021.11.030.

Yang, G., Lee, K., Lee, M.-H., Kim, S.-H., Ham, I.-H., Choi, H.-Y., 2011. Inhibitory effects of *Chelidonium majus* extract on atopic dermatitis-like skin lesions in NC/Nga mice. J. Ethnopharmacol. 138, 398–403. https://doi.org/10.1016/j.jep.2011.09.028.

Yargholi, A., Shirbeigi, L., Rahimi, R., Mansouri, P., Ayati, M.H., 2021. The effect of Melissa officinalis syrup on patients with mild to moderate psoriasis: a randomized, double-blind placebo-controlled clinical trial. BMC. Res. Notes 14, 253. https://doi.org/10.1186/s13104-021-05667-9.

Ye, L., Gao, Y., Mok, S.W.F., Liao, W., Wang, Y., Chen, C., Yang, L., Zhang, J., Shi, L., 2024. Modulation of alveolar macrophage and mitochondrial fitness by medicinal plant-derived nanovesicles to mitigate acute lung injury and viral pneumonia. J. Nanobiotechnol. 22, 190. https://doi.org/10.1186/s12951-024-02473-w.

Yu, C., Liu, Y., Yu, X., Liu, J., Cao, P., Liu, G., Cai, Y., Zhang, Y., Luan, Q., 2025. Garlic-Derived Exosome-Like Nanovesicles: a Promising Natural Nanotherapy for Periodontitis via PHGDH/PI3K/AKT-Mediated Metabolic and Inflammatory Regulation. Int. J. Nanomedicine 20, 5551–5572. https://doi.org/10.2147/IJN.S510417.

Yücel, A., Kan, Y., Yesilada, E., Akın, O., 2017. Effect of St.John's wort (*Hypericum perforatum*) oily extract for the care and treatment of pressure sores; a case report. J. Ethnopharmacol. 196, 236–241. https://doi.org/10.1016/j.jep.2016.12.030.

Yun, C., Jung, Y., Chun, W., Yang, B., Ryu, J., Lim, C., Kim, J.-H., Kim, H., Cho, S.-I., 2016. Anti-inflammatory effects of artemisia leaf extract in mice with contact dermatitis in vitro and in vivo. Mediators. Inflamm. 2016, 8027537. https://doi.org/10.1155/2016/8027537.

Zhang, B., Alysandratos, K.-D., Angelidou, A., Asadi, S., Sismanopoulos, N., Delivanis, D.-A., Weng, Z., Miniati, A., Vasiadi, M., Katsarou-Katsari, A., Miao, B., Leeman, S.E., Kalogeromitros, D., Theoharides, T.C., 2011. Human mast cell degranulation and preformed TNF secretion require mitochondrial translocation to exocytosis sites: relevance to atopic dermatitis. J. Allergy Clin. Immunol. 127, 1522–1531. https://doi.org/10.1016/j.jaci.2011.02.005. .e8.

Zhang, L., Ji, L., Tang, X., Chen, X., Li, Z., Mi, X., Yang, L., 2015. Inhibition to DRP1 translocation can mitigate p38 MAPK-signaling pathway activation in GMC induced by hyperglycemia. Ren. Fail. 37, 903–910. https://doi.org/10.3109/0886022X.2015.1034607.